Computers and Fluids 220 (2021) 104884

Contents lists available at ScienceDirect

Computers and Fluids

journal homepage: www.elsevier.com/locate/compfluid

Diffuse bounce back condition for lattice Boltzmann method

Geng Liu, Taehun Lee*

Department of Mechanical Engineering, The City College of New York, New York, NY 10031, USA

ARTICLE INFO

Article history:
Received 13 September 2020
Revised 29 January 2021
Accepted 12 February 2021
Available online 23 February 2021

Keywords:
Diffuse bounce back
Boundary condition
Lattice Boltzmann method

ABSTRACT

The lattice Boltzmann method has been widely used in curved and moving boundary fluid simulations. Both explicit and implicit treatments are studied to recover proper boundary conditions on Cartesian grids. These methods can describe curved boundaries more accurately and more smoothly than the staircase approximation. However, to improve the order of accuracy and to reduce the fluctuation of force, complicated modifications have been applied to the collision step of lattice Boltzmann equation. In this study, a new boundary scheme based on diffuse geometry is proposed for lattice Boltzmann method. The scheme is derived by directly incorporating the bounce back condition into the weak form of the streaming step of discretized Boltzmann equation. The new method does not change the collision operator. Therefore it can be easily combined with complex collision models. Although diffuse boundary is introduced, this scheme recovers exact bounce back condition at sharp boundary limit, regardless of the shapes and motions of the boundaries. Numerical tests show that the accuracy of this method is second order and depends on the boundary thickness and several other factors. In moving boundary problems, the fluctuation of force can be largely reduced compared to popular sharp boundary conditions because it does not require extrapolation to fulfil the unknown information of the newly generated fluid nodes around the boundaries. In this paper the detailed derivation for the new scheme is explained and the benchmark problems are solved to test its accuracy and the effect of different parameters.

1. Introduction

The lattice Boltzmann method (LBM) has become very popular in simulating fluids. However, the original LBM is implemented on uniform Cartesian grids and hence naturally weak in solving curved boundary and moving boundary problems. These problems are interesting to researchers since fluid-solid interaction and the dynamics of suspension are commonly seen in fluid simulations.

Bounce back is the most popular and typical explicit boundary condition for no-slip boundaries in LBM, however it can only deal with straight boundaries that are parallel to the grid lines. In early simulations curved boundaries are represented by staircases so that simple bounce back can be applied. The staircases not only bring inaccuracy into the system, but also generate small vortices when Reynolds number is large. A variety of methods have been investigated to recover curved boundaries in LBM. These methods in general can be classified into interpolated schemes, diffuse schemes and immersed boundary schemes (a special case of diffuse schemes). Filippova-Hänel scheme [1,2] is one of the first interpolated boundary schemes. It constructs a virtual equilibrium probability distribution function (PDF), and calculates the incoming PDFs with extrapolation. In 2001, Bouzidi et al. [3] combined the basic halfway linking bounce back condition with interpolation. Lallemand and Luo [4] further extend the scheme to moving boundary cases. These and most other interpolated schemes can recover sharp boundaries, yet they have apparent weaknesses. Besides the numerical instability introduced by the interpolation schemes, the force fluctuation is obvious [5,6].

Inspired by Peskin [7,8] and many others, the Immersed Boundary Method (IBM) has been applied to LBM [9–12]. Although IBM was invented to solve membrane problems, it can tackle with rigid body problems if the stiffness of the boundary is increased to a large value. The original Immersed Boundary lattice Boltzmann method (IB-LBM) [9] was based on penalty force model directly inherited from Navier-Stokes governed IBM. Later it was discovered that the enforcement for boundary can be recovered by directly taking the momentum exchange in LBM [11,12]. This development eliminated the need of user defined penalty parameters. Inamuro further extended the method to two phase flow problems [13]. IB-LBM avoids interpolation in moving boundary problems and it reduces the fluctuation of force and velocity. However, the IB-LBM approaches usually require a set of Lagrangian

* Corresponding author.
E-mail address: thlee@ccny.cuny.edu (T. Lee).

https://doi.org/10.1016/j.compfluid.2021.104884
0045-7930/

boundary nodes independent of the Eulerian grid, while the order of their accuracies remains the same as other diffuse boundary conditions.

Like in IBM, normal diffuse boundary conditions also describe the geometry with a smooth order parameter. Partially Saturated Method (PSM) [14], as one kind of implicit boundary condition, allows for smooth shift from pure fluid to solid obstacles by introducing a partially saturated collision operator. The nature of PSM is to add penalty force to the distributions, which comes out to be the same idea as some porous media models. One benefit of smooth shift is that no extrapolations are required for the moving boundary problems. However, according to the model of Noble et al., the no-slip condition cannot be perfectly recovered, what they recover at sharp boundary limit is actually Zou-He Dirichlet boundary condition [15]. More recently, Krause et al. proposed a homogenised scheme [16]. In Krause's model, the penalty force is replaced with additional momentum generated by direct combination of local fluid velocity and no-slip boundary condition on the basis of partially saturated parameter. In this way the boundary velocity converge to the imposed condition at sharp boundary limit. The boundary force in implicit models can in general be calculated by taking the first moment of the extra momentum. Apart from the advantages, both methods has only one order parameter that controls the behaviors of all the directions on the boundary node. This treatment does not distinguish the distributions by the angles formed by their directions and the local boundary normal vector. In the directions that are close to the tangent direction of the boundary, more streaming should be allowed. The modification for collision step should be carefully associated with other models when applied to complex problems. Like most diffuse methods, the above two boundary conditions are first order accurate.

It is difficult to get rid of all the listed flaws of different methods at the same time. In this paper a new diffuse boundary condition for LBM is proposed. Although penetration cannot be completely avoided, diffuse methods can be easily applied to curved and moving boundary problems. The derivation of this method is inspired by Li et al.'s derivation [17] and Aland et al.'s work [18]. In their work diffuse geometries are introduced and boundary conditions are incorporated into the governing equations. Unlike in [18] where the Navier-Stokes equation is combined with no slip condition, the associated boundary condition for LBM is nodal bounce back. The reason why halfway linking bounce back is selected is that in the derivation boundary conditions should be applied exactly to the boundary positions. The new method is named Diffuse Bounce Back-Lattice Boltzmann Method (DBB-LBM). At sharp boundary limit DBB-LBM recovers the bounce back condition. Like other implicit schemes, DBB-LBM has a smooth boundary and can simulate curved boundary problems without employing interpolation or extrapolation. In moving boundary problems solved with DBB-LBM, the force fluctuation caused by discontinuity can also be significantly reduced if the scheme is applied properly. More importantly, DBB-LBM is a modification of propagation step. Different collision models for complex physics can be directly inserted into the solver because collision does not affect the incorporated boundary condition.

In the following sections, DBB-LBM is introduced and tested in detail. Section 2 explains how DBB-LBM is derived and discretized. In Section 3, the new scheme is validated by several benchmark problems. The convergence of the fluid field and the effect of some parameters are discussed with a Taylor Couette flow example. The force evaluation is validated with a 2D cylinder flow problem. The example of impulsively started cylinder in a channel shows Galilean invariance and how DBB-LBM manages the boundary force fluctuation. Section 4 concludes the features of DBB-LBM.

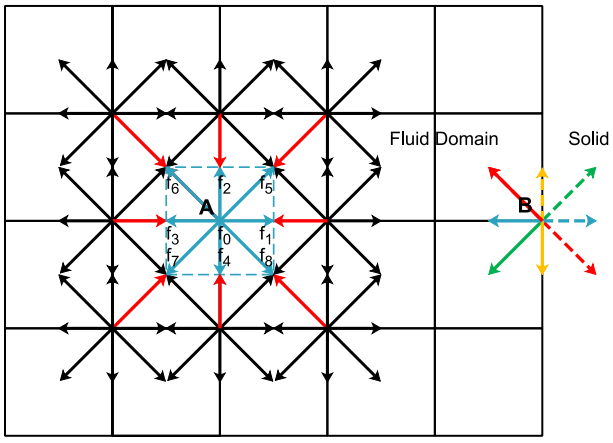

Fig. 1. D2Q9 model.

2. Derivation of the diffuse bounce back lattice Boltzmann equations

The DBB-LBM is derived from discretizing the bounce-back-incorporated discrete Boltzmann equations (DBEs). The process of inserting the bounce back boundary condition and the discretization of the DBE are explained in this section. While LBM consists of two major steps, collision and streaming, The boundary condition is only applied to the streaming process because collision algorithm is usually local. The extra momentum caused by the boundary condition is also an important ingredient for evaluating the boundary forces.

2.1. Lattice Boltzmann equation

The lattice Boltzmann method simulates fluids by iteratively repeating the collision and streaming of particle distribution functions (PDFs). The collision and streaming steps for force free fluid in their general forms [19] can be written as

$$\begin{aligned} &\text{collision:}\quad \mathbf{f}^{*} = \mathbf{f} - \mathbf{M}^{-1}\mathbf{S}\mathbf{M}(\mathbf{f} - \mathbf{f}^{\mathrm{eq}}),\\ &\text{streaming:}\quad f_{\alpha}(\mathbf{x}, t) = f_{\alpha}^{*}(\mathbf{x} - \mathbf{e}_{\alpha}\delta_t, t - \delta_t)\\ &\qquad\qquad \text{in } \Omega \text{ for } \alpha = 0, 1, \ldots, N_{\alpha} - 1, \end{aligned} \tag{1}$$

where $\mathbf{f}$ is the vector form of PDFs, $\mathbf{f}^{\mathrm{eq}}$ is the equilibrium PDF vector that can be defined by specific LB models, $\mathbf{f}^{*}$ is the post-collision PDF vector. $\mathbf{M}$ is the matrix that transforms the distributions to the moment space where collision is defined, and the diagonal matrix $\mathbf{S}$ is the relaxation frequency matrix. If the single-relaxation-time (SRT) collision model [20] is employed, the relaxation frequencies are related to the kinematic viscosity in the same way $s = \delta_t/(\nu/c_s^2 + 0.5\delta_t)$, where ν is the kinematic viscosity, and c_s is the speed of sound. f_{α} is the PDF in the direction of the lattice velocity $\mathbf{e}_{\alpha}$, $\mathbf{x}$ is the position of a certain node in the discretized fluid domain, t is the time and δ_t is the time increment. N_{α} is the number of lattice velocities, and Ω is the fluid domain. Note that for convenience $f_{\alpha}(\mathbf{x}, t)$ is denoted by $f_{\alpha}|_{\mathbf{x}}^{t}$ hereafter.

The most typical 2-dimension-9-velocity model (D2Q9) of LBM can be depicted by Fig. 1 [21]. N_{α} in this case is 9. On the fluid node A, the collision step is executed locally and in the streaming step, the red neighboring distributions are advected to node A in the corresponding directions.

According to the incompressible model [22–24], the equilibrium distribution f_{α}^{eq} is expressed by

$$f_{\alpha}^{\mathrm{eq}} = t_{\alpha}\left[\frac{p}{c_s^2} + \rho_0\left(\frac{\mathbf{e}_{\alpha}\cdot\mathbf{u}}{c_s^2} + \frac{(\mathbf{e}_{\alpha}\cdot\mathbf{u})^2}{2c_s^4} - \frac{\mathbf{u}\cdot\mathbf{u}}{2c_s^2}\right)\right], \tag{2}$$

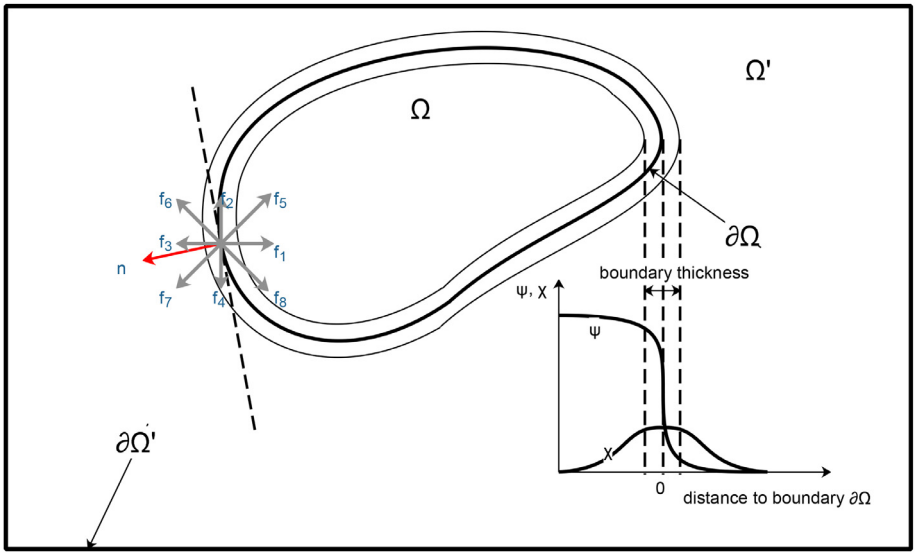

Fig. 2. The diffuse geometry of Ω.

where ρ_0 is density, $\mathbf{u}$ is velocity, p is pressure, t_α is the corresponding weight and $c_s = \delta_x/(\sqrt{3}\delta_t)$, δ_x is the grid size. The macroscopic physical properties of the fluid can be recovered by taking the moments of the PDFs,

$$p = c_s^2 \sum_{\alpha=0}^{N_\alpha - 1} f_\alpha, \quad \rho_0 \mathbf{u} = \sum_{\alpha=0}^{N_\alpha - 1} \mathbf{e}_\alpha f_\alpha. \tag{3}$$

The DBE is the continuous form of lattice Boltzmann equation. According to the Strang splitting [25,26] technique, the DBE in a discrete time step can be described by the following equation

$$f_\alpha^{n+1} = C(\delta_t/2) \circ S(\delta_t) \circ C(\delta_t/2) f_\alpha^n, \tag{4}$$

where the elapsed time between f_α^n and f_α^{n+1} is δ_t, C is the collision operator in Eq. (1) and S is the streaming operator with boundary condition. To be more specific, S is the operator for numerically solving the following partial differential equation

$$\frac{\partial f_\alpha}{\partial t} + \nabla \cdot (\mathbf{e}_\alpha f_\alpha) = 0. \tag{5}$$

Besides Eq. (5), another important ingredient for deriving the DBB-LBM is the bounce back boundary condition. Bounce back for straight no-slip boundaries is also shown in Fig. 1. On node B, the outgoing distributions are in dashed lines. The result of bounce back is that an outgoing PDF is reflected to the corresponding incoming PDF with the same color in solid line. The bounce back process can be mathematically expressed by

$$f_\alpha = f_{\bar{\alpha}} + 2t_\alpha \rho_0 (\mathbf{e}_\alpha \cdot \mathbf{u}_b)/c_s^2, \tag{6}$$

where $f_{\bar{\alpha}}$ and f_α are in opposite directions and $\mathbf{u}_b$ is imposed boundary velocity.

2.2. Derivation of diffuse bounce back discrete Boltzmann equation

The derivation of DBB-DBE starts from taking the weak form of Eq. (5)

$$\int_\Omega \lambda \left[\frac{\partial f_\alpha}{\partial t} + \nabla \cdot (\mathbf{e}_\alpha f_\alpha) \right] d\mathbf{x} = 0, \tag{7}$$

where λ is an arbitrary function. Applying integration by parts to Eq. (7), we have

$$\int_{\partial\Omega} \lambda f_\alpha (\mathbf{e}_\alpha \cdot \mathbf{n}) d\mathbf{x} - \int_\Omega (\nabla\lambda \cdot \mathbf{e}_\alpha) f_\alpha d\mathbf{x} = -\int_\Omega \lambda \frac{\partial f_\alpha}{\partial t} d\mathbf{x}, \tag{8}$$

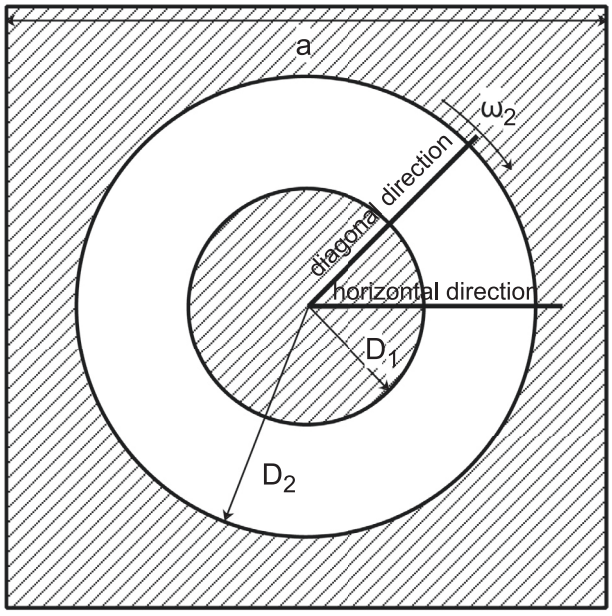

Fig. 3. Setup of Taylor Couette flow.

where $\partial\Omega$ is the boundary of Ω and $\mathbf{n}$ is the unit normal vector. After the bounce back boundary condition Eq. (6) is incorporated, the following equation should hold

$$\int_{\partial\Omega} \lambda (f_{\bar{\alpha}} + \eta_\alpha)(\mathbf{e}_\alpha \cdot \mathbf{n}) d\mathbf{x} - \int_\Omega (\nabla\lambda \cdot \mathbf{e}_\alpha) f_\alpha d\mathbf{x} = -\int_\Omega \lambda \frac{\partial f_\alpha}{\partial t} d\mathbf{x}, \tag{9}$$

where η_α denotes the imposed boundary velocity term $2t_\alpha \rho_0 (\mathbf{e}_\alpha \cdot \mathbf{u}_b)/c_s^2$ for convenience.

The geometry of Ω is described by a smooth phase order parameter ψ in the perspective of a larger domain Ω' that contains Ω (Fig. 2).

The profile of ψ is also shown in Fig. 2, it behaves like a switch for fluid and solid domains. Ideally ψ is 1 in the fluid phase and is 0 in the solid phase. However, a $\nabla\psi$ related parameter χ is required for identifying the boundary of Ω, a smooth profile for ψ should be used in practice. With ψ and χ the integrating domain of Eq. (9) can be changed to Ω' by multiplying activating parame-

ters to the integrant,

$$\int_{\Omega'} \chi\lambda(f_{\tilde{\alpha}}+\eta_\alpha)(\mathbf{e}_\alpha\cdot\mathbf{n})d\mathbf{x}-\int_{\Omega'}\psi f_\alpha(\nabla\lambda\cdot\mathbf{e}_\alpha)d\mathbf{x} =-\int_{\Omega'}\psi\lambda\frac{\partial f_\alpha}{\partial t}d\mathbf{x}. \tag{10}$$

Hyperbolic tangent function is a popular model for smooth boundary order parameters, because it is smooth and its derivative is good representation of boundary. So ψ and χ are expressed as

$$\psi=\frac{1+\tanh(2l/\epsilon)}{2},\quad \chi\mathbf{n}=-\nabla\psi, \tag{11}$$

where l is the distance to boundary, ϵ is the diffuse boundary thickness. Theoretically there is no sharp transition in both ψ and χ, so the force fluctuations in the moving boundary cases can be reduced. Other non-differentiable profiles may still have discontinuity in high order derivatives.

Since ψ goes to zero on $\partial\Omega'$, by applying integration by parts to Eq. (10), the integral form of the diffuse bounce back advection equation is obtained

$$\int_{\Omega'}\lambda\left[\nabla\cdot(\psi\mathbf{e}_\alpha f_\alpha)+\psi\frac{\partial f_\alpha}{\partial t}-(f_{\tilde{\alpha}}+\eta_\alpha)(\mathbf{e}_\alpha\cdot\nabla\psi)\right]d\mathbf{x}=0. \tag{12}$$

As defined λ is an arbitrary function, therefore the rest part of the integrant should be zero.

$$\frac{\partial f_\alpha}{\partial t}+\nabla\cdot(\mathbf{e}_\alpha f_\alpha)=\frac{\nabla\psi\cdot\mathbf{e}_\alpha}{\psi}(f_{\tilde{\alpha}}-f_\alpha+\eta_\alpha). \tag{13}$$

The above equation is valid in the large computational domain Ω'.

Derived from Eq. (11), the gradient of order parameter should be expressed by

$$\nabla\psi=\frac{4\psi(1-\psi)}{\epsilon}\mathbf{n}, \tag{14}$$

hence Eq. (13) can be rewritten as

$$\frac{\partial f_\alpha}{\partial t}+\nabla\cdot(\mathbf{e}_\alpha f_\alpha)=\frac{4(1-\psi)}{\epsilon}(\mathbf{n}\cdot\mathbf{e}_\alpha)(f_{\tilde{\alpha}}-f_\alpha+\eta_\alpha). \tag{15}$$

In direction α, such as the directions of f_3, f_4, f_6 and f_7 shown in Fig. 2, where $\mathbf{n}\cdot\mathbf{e}_\alpha\geqslant 0$, the boundary conditions are applied as they should be. However, bounce back is not applied to their opposite directions in the bulk of solid. In direction α where $(\mathbf{n}\cdot\mathbf{e}_\alpha)$ is smaller than 0, ζ_α should not function, therefore the product $(\mathbf{n}\cdot\mathbf{e}_\alpha)$ in this direction is set to 0. $\mathbf{n}\cdot\mathbf{e}_\alpha$ in Eq. (15) must be replaced by the maximum of $\mathbf{n}\cdot\mathbf{e}_\alpha$ and 0.

$$\frac{\partial f_\alpha}{\partial t}+\nabla\cdot(\mathbf{e}_\alpha f_\alpha)=\frac{4(1-\psi)}{\epsilon}\max(\mathbf{n}\cdot\mathbf{e}_\alpha,0)(f_{\tilde{\alpha}}-f_\alpha+\eta_\alpha). \tag{16}$$

Denoting $4(1-\psi)\max(\mathbf{n}\cdot\mathbf{e}_\alpha,0)/\epsilon$ by ζ_α, the diffuse bounce back advection equation (Eq. (17)) can be obtained.

$$\frac{\partial f_\alpha}{\partial t}+\nabla\cdot(\mathbf{e}_\alpha f_\alpha)=\zeta_\alpha(f_{\tilde{\alpha}}-f_\alpha+\eta_\alpha). \tag{17}$$

Note that ζ_α varies with the distribution directions. This makes the penalty effect dependant on the directions. The propagation of incoming distributions in the boundary tangent line directions is degenerated to traditional lattice Boltzmann propagation, and the extra term for recovering bounce-back condition is applied to normal directions the most.

2.3. Discretization of the diffuse bounce back propagation equation

To discretize Eq. (17), both sides of the equation are integrated over time period $[t-\delta_t,t]$ with coupled space integration limits $[\mathbf{x}-\mathbf{e}_\alpha\delta_t,\mathbf{x}]$,

$$f_\alpha|^t_{\mathbf{x}}-f_\alpha|^{t-\delta_t}_{\mathbf{x}-\mathbf{e}_\alpha\delta_t}=\int_{t-\delta_t}^{t}\zeta_\alpha(f_{\tilde{\alpha}}-f_\alpha+\eta_\alpha)dt. \tag{18}$$

The right hand side of the Eq. (18) is numerically evaluated,

$$f_\alpha|^t_{\mathbf{x}}-f_\alpha|^{t-\delta_t}_{\mathbf{x}-\mathbf{e}_\alpha\delta_t} =\delta_t\left[\theta\,\zeta_\alpha|^t_{\mathbf{x}}(f_{\tilde{\alpha}}-f_\alpha+\eta_\alpha)|^t_{\mathbf{x}}+(1-\theta)\,\zeta_\alpha|^{t-\delta_t}_{\mathbf{x}-\mathbf{e}_\alpha\delta_t}(f_{\tilde{\alpha}}-f_\alpha+\eta_\alpha)|^{t-\delta_t}_{\mathbf{x}-\mathbf{e}_\alpha\delta_t}\right]. \tag{19}$$

The parameter θ suggests different numerical schemes. $\theta=0.5$ means Crank-Nicolson scheme and $\theta=1$ implies implicit Euler scheme.

Eq. (19) is coupled with the same equation in the opposite direction. By decoupling the two equations, the discretized propagation step for DBB-LBM is obtained as

$$\begin{aligned}f_\alpha|^t_{\mathbf{x}} =\ & f_\alpha|^{t-\delta_t}_{\mathbf{x}-\mathbf{e}_\alpha\delta_t}+\frac{c_1}{c_0}\left(f_{\tilde{\alpha}}|^{t-\delta_t}_{\mathbf{x}+\mathbf{e}_\alpha\delta_t}-f_\alpha|^{t-\delta_t}_{\mathbf{x}-\mathbf{e}_\alpha\delta_t}+\eta_\alpha|^t_{\mathbf{x}}\right)\\ &+\frac{(1+c_2)c_3}{c_0}(f_{\tilde{\alpha}}-f_\alpha+\eta_\alpha)|^{t-\delta_t}_{\mathbf{x}-\mathbf{e}_\alpha\delta_t}\\ &-\frac{c_1c_4}{c_0}(f_{\tilde{\alpha}}-f_\alpha+\eta_\alpha)|^{t-\delta_t}_{\mathbf{x}+\mathbf{e}_\alpha\delta_t},\end{aligned} \tag{20}$$

where the c_0 to c_4 are coefficients related to ζ

$$\begin{aligned}&c_0=1+c_1+c_2,\quad c_1=\delta_t\theta\,\zeta_\alpha|^t_{\mathbf{x}},\quad c_2=\delta_t\theta\,\zeta_{\tilde{\alpha}}|^t_{\mathbf{x}}\\ &c_3=\delta_t(1-\theta)\,\zeta_\alpha|^{t-\delta_t}_{\mathbf{x}-\mathbf{e}_\alpha},\quad c_4=\delta_t(1-\theta)\,\zeta_{\tilde{\alpha}}|^{t-\delta_t}_{\mathbf{x}+\mathbf{e}_\alpha}.\end{aligned} \tag{21}$$

In the implicit Euler case, the DBB-LBM propagation has a simple form,

$$f_\alpha|^t_{\mathbf{x}}=f_\alpha|^{t-\delta_t}_{\mathbf{x}-\mathbf{e}_\alpha\delta_t}+\frac{c_1}{c_0}\left(f_{\tilde{\alpha}}|^{t-\delta_t}_{\mathbf{x}+\mathbf{e}_\alpha\delta_t}-f_\alpha|^{t-\delta_t}_{\mathbf{x}-\mathbf{e}_\alpha\delta_t}+\eta_\alpha|^t_{\mathbf{x}}\right). \tag{22}$$

It is interesting to note that Eq. (22) can be separated into two steps, the normal propagation step and a local operation.

$$\begin{aligned}f^{**}_\alpha|^t_{\mathbf{x}} &= f^{*}_\alpha|^{t-\delta_t}_{\mathbf{x}-\mathbf{e}_\alpha\delta_t},\\ f_\alpha &= f^{**}_\alpha+\frac{c_1}{c_0}\left(-f^{**}_\alpha+f^{**}_{\tilde{\alpha}}+\eta_\alpha\right).\end{aligned} \tag{23}$$

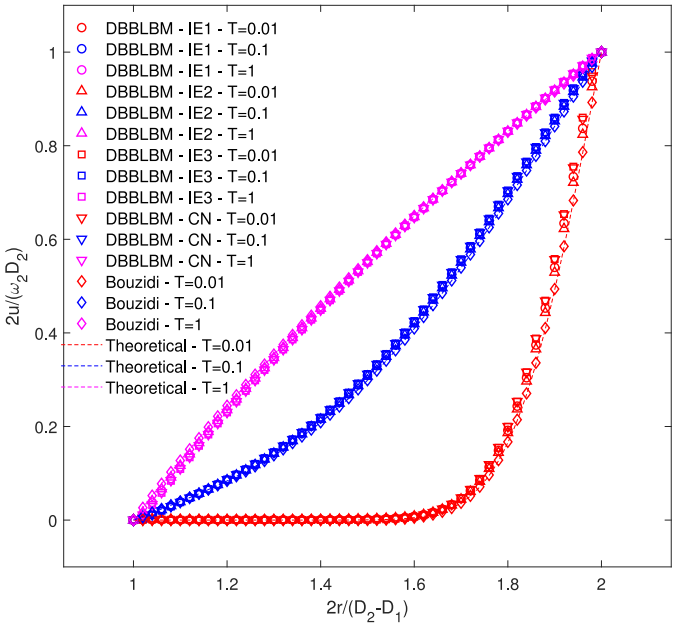

Fig. 4. Transient solutions for Taylor Couette flow velocity. IE1, IE2 and IE3 are Implicit Euler schemes, and CN is Crank Nicolson scheme. IE1, IE2 and IE3 corresponds to analytical ζ, biased difference ζ and central difference ζ respectively. The dashed lines are analytical solutions. Red, blue and magenta colors represent solutions at $T=0.01$, $T=0.1$ and $T=1$. r is the distance to the circle center. (For interpretation of the references to colour in this figure legend, the reader is referred to the web version of this article.)

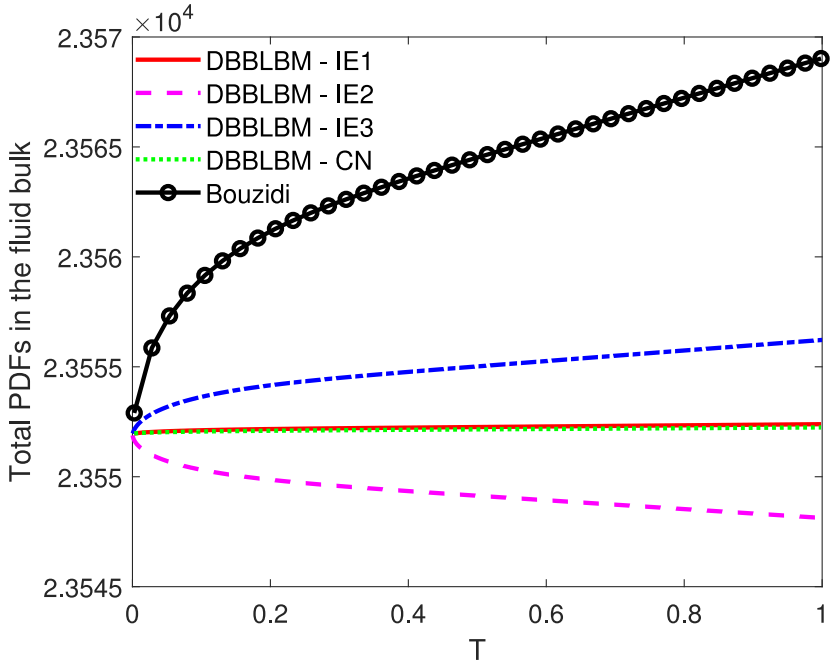

Fig. 5. Total fluid bulk PDF conservation. IE1, IE2, IE3 and CN are the same meaning as in Fig. 4.

3. Validation and application

In this section, test cases are solved with DBB-LBM. The Taylor Couette flow example is a validation for the accuracy of velocity. The accuracy not only depends on the resolution, but also the boundary thickness and how the DBE is discretized. The results can suggest how to choose the scheme and parameters. The drag coefficient of cylinder flow is then studied to test the validity of force calculation. An unsteady cylinder flow is employed to test the Galilean invariance feature of DBB-LBM. This simulation is implemented in two ways, moving frame and stationary frame. Ideally, the results of the two cases should be identical. Like other implicit boundary conditions, DBB-LBM can largely reduce the force noise in the stationary frame case if applied properly.

3.1. Taylor Couette flow

The setup of Taylor Couette flow is depicted in Fig. 3. The computational domain is a square with side length a, and the fluid domain is between the two concentric circles. The diameters of the circles are $D_1 = 25a/64$ and $D_2 = 2D_1$. The characteristic length is the difference between the radii of outer and inner circles. The

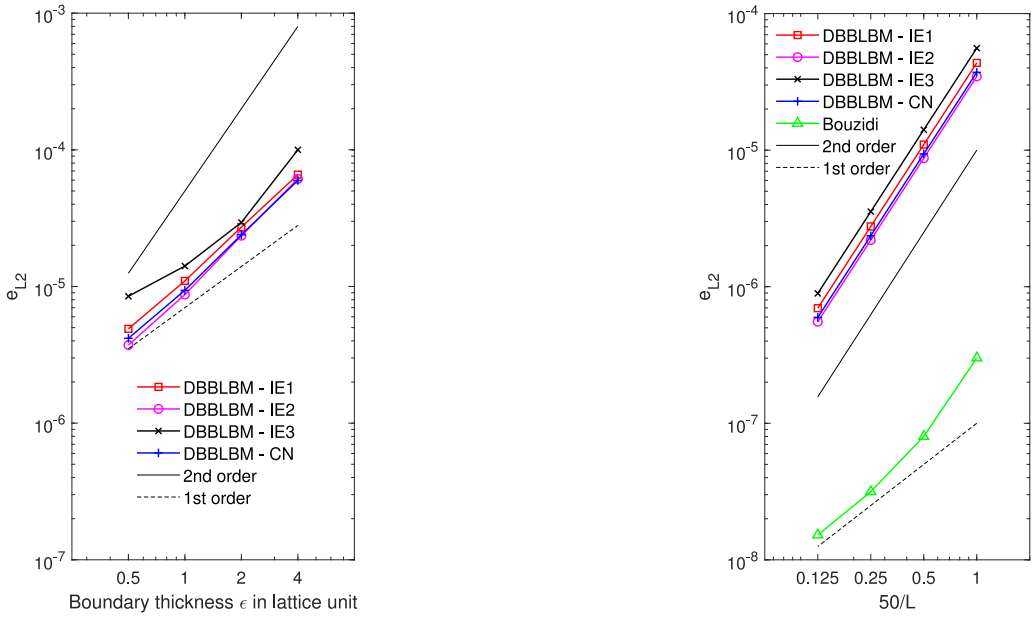

(a) Influence of boundary thickness ϵ to different DBB-LBM schemes. IE1, IE2, IE3 and CN are the same meaning as in Fig. 4.

(b) Convergence of different DBB-LBM schemes as mesh is refined. IE1, IE2, IE3 and CN are the same meaning as in Fig. 4.

Fig. 6. Convergence tests for DBB-LBM schemes.

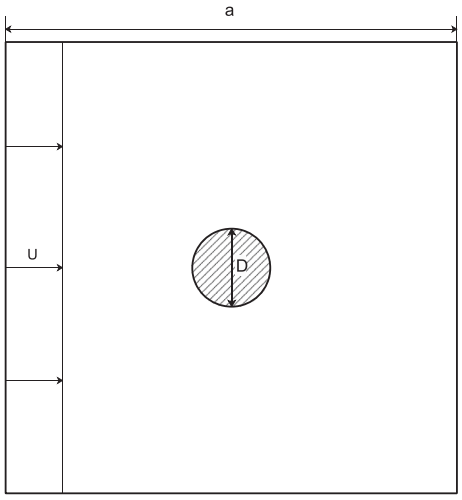

Fig. 7. Setup of 2D cylinder flow.

outer circle rotates with an angular velocity ω_2 while the inner wall remains stationary. The Reynolds number is 45. At this Reynolds number, SRT collision model works well, hence the relaxation frequencies in matrix $\mathbf{S}$ are set to the same value. The kinematic viscosity ν is 0.032, and the initial angular velocity for the outer circle is $\omega_2 = 4\nu\mathrm{Re}/(D_2 - D_1)/D_2$. The boundary thickness ϵ is 1 in lattice unit.

Since the outer circle rotates with a constant angular velocity, the direction of the imposed velocity varies along the boundary. In this case the exact value of the imposed velocity at the nodes off the $\psi = 0.5$ contour line cannot be determined without a reasonable definition. The one way to define imposed velocity for the off boundary nodes is to copy the imposed wall velocity in or opposite to the normal direction of the current node. This treatment assumes that the gradient of the imposed velocity in the normal direction is 0. The gradient has a significant impact on the boundary vicinity solutions. Unless the expected solution for velocity is also gradient free on the boundary, the preceding definition should generate a non-negligible boundary error. What's more, an inconsistency of this definition is that it does not satisfy the continuum equation. Although the imposed velocities on off boundary nodes contribute more to the boundary velocity than the bulk velocity, such inconsistency had better be avoided. Fortunately there is a simpler definition that can fix the defects. Since the effect of local imposed velocity to the boundary condition is weakened as the inspected node gets farther away from the boundary, non-zero boundary velocities are only required in a relatively narrow band around the outer circle. Inside this band the local imposed velocity can be expressed by $\mathbf{u}_b = (x - x_c, y - y_c)\omega_2$, where (x, y) is the position of the node and (x_c, y_c) is the center of circle, meaning that a fixed angular velocity is imposed around the boundary. The magnitude of the imposed velocity varies in the radial direction, but the difference can be neglected since the boundary band is narrow. This definition looks like treating the boundary band as a rigid body, yet it is not true because the imposed velocities inside the band contribute more to the real boundary, instead of its neighborhood.

In this test case, the propagation step is discretized with both Crank-Nicolson scheme and Implicit Euler scheme. In the Implicit Euler scheme, the coefficient ζ_α can be obtained in three ways, analytical solution, biased difference and central difference. The detailed expressions are as follows,

$$\text{Analytical solution:} \quad \zeta_\alpha|_{\mathbf{x}} = \frac{4(1 - \psi|_{\mathbf{x}})}{\epsilon}\max(\mathbf{n}\cdot\mathbf{e}_\alpha, 0), \tag{24}$$

$$\text{Biased difference:} \quad \zeta_\alpha|_{\mathbf{x}} = \frac{\max(\psi|_{\mathbf{x}+\mathbf{e}_\alpha\delta_t} - \psi|_{\mathbf{x}}, 0)}{\delta_x \psi|_{\mathbf{x}}}, \tag{25}$$

$$\text{Central difference:} \quad \zeta_\alpha|_{\mathbf{x}} = \frac{\max(\psi|_{\mathbf{x}+\mathbf{e}_\alpha\delta_t} - \psi|_{\mathbf{x}-\mathbf{e}_\alpha\delta_t}, 0)}{2\delta_x \psi|_{\mathbf{x}}}. \tag{26}$$

The performance of these schemes are shown in Fig. 4. The transient solutions for the magnitude of velocity along the radial direction are plotted. The characteristic length is $L = (D_2 - D_1)/2 = 50$. The transient solutions for $T = 0.01$, $T = 0.1$ and $T = 1$ are plotted on the graph, while $T = \nu t/L^2$ is the normalised time. At $T = 1$, the solutions are close to steady state solution. From Fig. 4, we see that the Implicit Euler DBB-LBM scheme works better than the Crank Nicolson scheme. The Implicit Euler scheme imitates the fact that bounce back condition is usually applied after the streaming step. Among the Implicit Euler schemes, ζ_α evaluated by taking the biased difference generates more accurate solutions, because in this case both the evaluation of ζ_α and the application of bounce back take place halfway along the characteristics.

In Fig. 4, the DBB-LBM are further compared with the Bouzidi method [3]. As Bouzidi is sharp boundary condition, the numerical solutions generated by this method agree very well with the analytical solution. On the other hand, in DBB-LBM, as explained previously, the errors in the neighborhood of the boundary are dependent to the gradient of the imposed velocity. For $T = 0.01$, the expected gradient of velocity near the outer circle is larger than the gradient of imposed velocity; while for $T = 1$, the expected

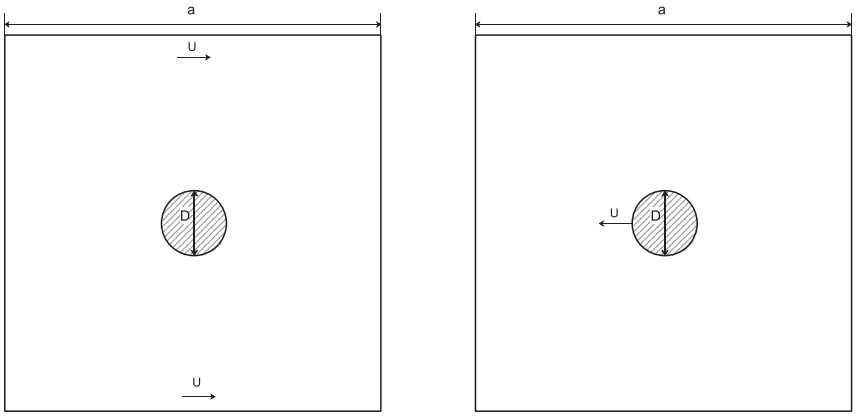

(a) Setup of moving frame flow. (b) Setup of stationary frame flow.

Fig. 8. Setup of moving frame and stationary frame cylinder flows.

gradient near the inner circle is also larger than the imposed gradient, which is 0. Such errors are commonly seen in diffuse boundary methods and can be avoided to a decent extent by adjusting the imposed boundary velocity distribution or refining the mesh.

Although as a diffuse boundary approach, DBB-LBM does not recover sharp boundary perfectly, it still inherits the features of bounce back boundary condition, and conserves the total PDFs in the fluid bulk much better than the Interpolated Bounce Back method like Bouzidi condition (Fig. 5). In Fig. 5, the change rates of total fluid bulk PDF for DBB-LBM schemes are smaller than that for the Bouzidi method. Analytical ζ performs the best in conserving the total fluid bulk PDF. Although Crank Nicolson scheme may introduce additional PDFs to the system, it came out to have slightly better conservation feature.

The influence of boundary thickness ϵ to the solution is important for diffuse boundary methods. For DBB-LBM we study this influence with the Taylor Couette flow application on a 512 by 512 grid, i.e. the characteristic length L is 100 in lattice unit. The steady state numerical solutions are assessed by taking the L-2 relative error e_{L2} defined in the following way,

$$e_{L2} = \frac{\sqrt{\sum_{(i,j)\in\Omega} \left(u_n(i,j) - u_t(i,j)\right)^2}}{N}, \tag{27}$$

where (i, j) represents the grid point, N is the number of grid points in the fluid bulk, u_n is the numerical solution for normalised velocity magnitude and u_t is the true value for the normalised velocity magnitude. For Taylor Couette flow, there is analytical solution for the normalised velocity magnitude,

$$u_t(r) = \frac{r/D_1 - (4r/D_1)^{-1}}{1 - (D_2/D_1)^{-2}}, \tag{28}$$

where u_t is expressed as a function of radius r and $D_1/2 \leqslant r \leqslant D_2/2$. The effects of boundary thickness for different schemes are shown in Fig. 6a. The orders of convergence for most DBB-LBM schemes lie in between first order and second order. The behavior of Implicit Euler scheme with central difference ζ becomes worse as the boundary thickness get smaller. This caused by the failure of recovering the gradient of ψ when the thickness ϵ is comparable or smaller than the grid size.

The quantified error analysis is further extended to its dependence on the resolution. The boundary thickness is fixed to 1, and the velocity errors under different resolutions ($L = 50,\ 100,\ 200,\ 400$) are plotted in Fig. 6b. The convergence rates for all DBB-LBM schemes in the inspected range are second order. Implicit Euler scheme with biased difference ζ produces the smallest absolute error. The schemes are also compared with Bouzidi method. Although Bouzidi method as a sharp boundary method is more accurate, the convergence rate can be reduced to first order as the mesh is refined to $L = 400$.

3.2. 2D cylinder flow

The boundary force can be evaluated by momentum exchange. In this section, the 2D cylinder flow is solved with DBB-LBM to test the behavior of drag coefficient. The setup is depicted by Fig. 7. D is the diameter of the cylinder at the center of the square domain, and $D = a/16$. Upper,lower and right walls of the domain are open boundaries. The profile of incoming flow velocity U is uniform and the pressure distribution on the left boundary is also fixed. The cylinder flow is simulated at Reynolds number $\mathrm{Re} = 20$, and the

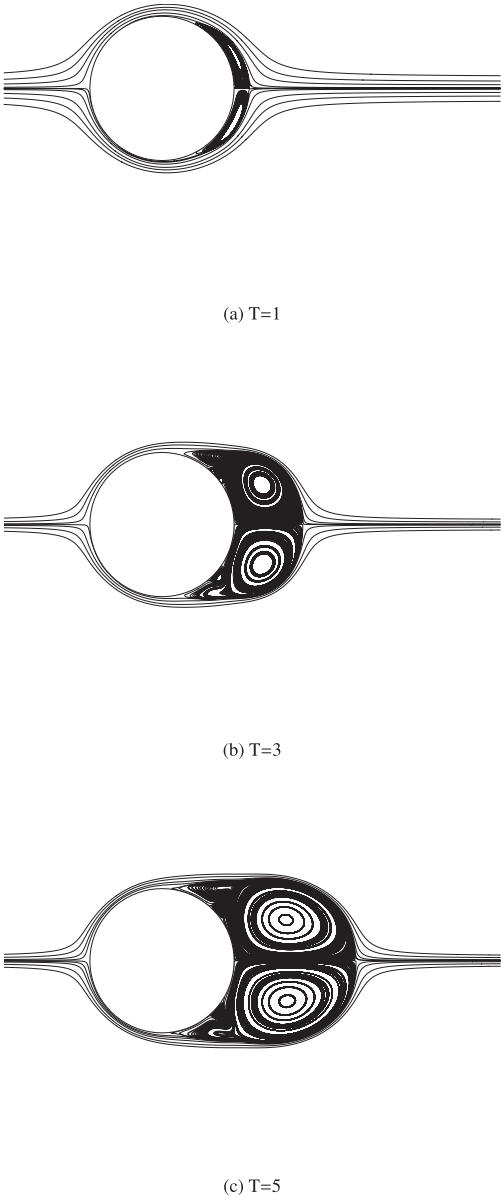

(a) T=1

(b) T=3

(c) T=5

Fig. 9. Time evolutions of streamlines at $Re = 550$ for moving frame and stationary frame cases using biased difference ζ_α and boundary thickness $\epsilon = 1$. (a) $T = 1$, moving frame (upper half), stationary frame (lower half); (b) $T = 3$, moving frame (upper half), stationary frame (lower half); (c) $T = 5$, moving frame (upper half), stationary frame (lower half).

Table 1
Drag coefficient C_D obtained with DBB-LBM under different resolutions and boundary thicknesses.

ϵ in lattice unit	1	2	3	4	Authors	Reported C_D values
D=16, analytical ζ_α	2.5109	2.0455	1.8520	1.7260	Tritton [27]	2.22
D=32, analytical ζ_α	2.5315	2.0880	1.8987	1.7840	Fornberg [28]	2.00
D=64, analytical ζ_α	2.5526	2.1059	1.9171	1.8044	Calhoun [29]	2.19
D=16, biased difference ζ_α	2.2367	1.9562	1.7998	1.6932	Nieuwstadt and Keller [30]	2.053
D=32, biased difference ζ_α	2.3045	2.0038	1.8465	1.7476	He and Doolen [31]	2.152
D=64, biased difference ζ_α	2.3360	2.0292	1.8705	1.7719	Lee and Lin [32][a]	2.086

[a] AE/CI, CFL=0.5

kinematic viscosity ν is 0.184752, meaning the Mach number is 0.1 when $a = 1024$. The kinematic viscosity remains unchanged for different resolutions. And the initial state of the flow is defined as inviscid solution.

The normalized drag force C_D can be expressed by

$$C_D = \frac{2F_D}{\rho_0 U^2 D} \tag{29}$$

where F_D is the horizontal component of total force $\mathbf{F}$, which can be achieved by evaluating the spatial integral of weighted momentum exchange,

$$\mathbf{F} = \sum_{\mathbf{x}} \left[\sum_{\alpha} \psi \zeta_\alpha \mathbf{e}_\alpha (f_\alpha + f_{\tilde{\alpha}}) \right] \delta_x^3, \tag{30}$$

Following the experience in Section 3.1 that ζ_α calculated by biased difference has the best convergence performance and that the analytical ζ_α has the best conservation feature, here we take these two cases and only consider the Implicit Euler scheme. When ζ_α is a result of biased difference (Eq. (25)), the corresponding coefficient in Eq. (30) should be treated the same way:

$$\mathbf{F}\delta_t = \sum_{\mathbf{x}} \left[\sum_{\zeta_\alpha > 0} (\psi(\mathbf{x} + \mathbf{e}_\alpha \delta_t) - \psi(\mathbf{x})) \mathbf{e}_\alpha (f_\alpha + f_{\tilde{\alpha}}) \right] \delta_x^3. \tag{31}$$

According to numerical tests, diffuse bounce back schemes may lead to spatial fluctuations of the tangential component of the boundary force field in the solid bulk, and this can be the main source of error for momentum exchange force model. To avoid this phenomenon, a modified relaxation time is introduced to the system:

$$\frac{1}{\tau'} = \frac{1}{\tau} + \psi \left(\frac{1}{\tau_s} - \frac{1}{\tau} \right), \tag{32}$$

where $\tau = \nu / (c_s^2 \delta_t)$ is the original relaxation time, τ_s is 0.5 and is applied to the solid material, τ' is the mixed relaxation time, and the applied relaxation frequency is $s = 1/(\tau' + 0.5)$. With this modification the physical feature of fluid is not changed, however, the collision step in the solid parts is reduced to equilibrium distributions, and this helps to weaken the spatial fluctuation effect in the solid.

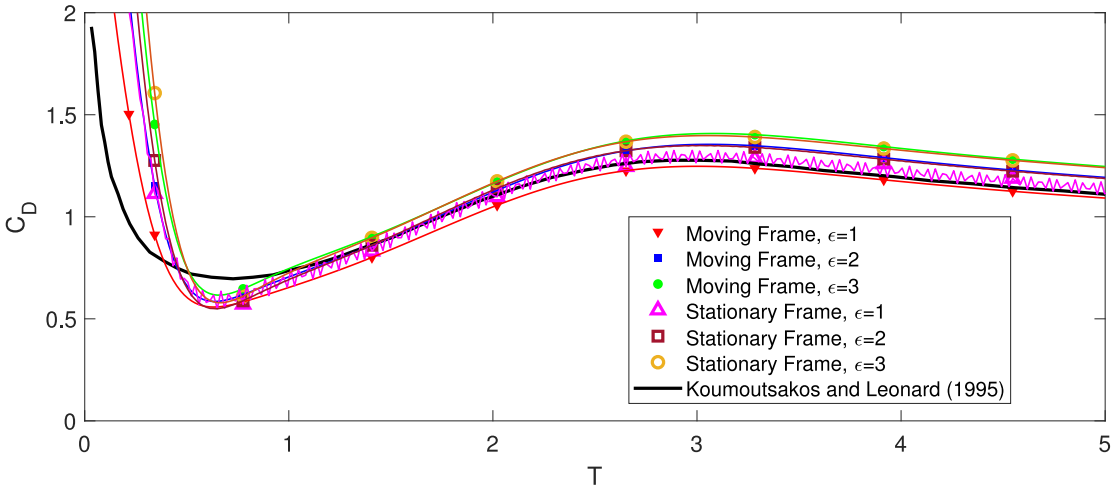

(a) C_D history of moving frame (solid symbols) and stationary frame (hollow symbols) cases with analytical ζ_α under different boundary thicknesses ($\epsilon = 1, 2, 3$).

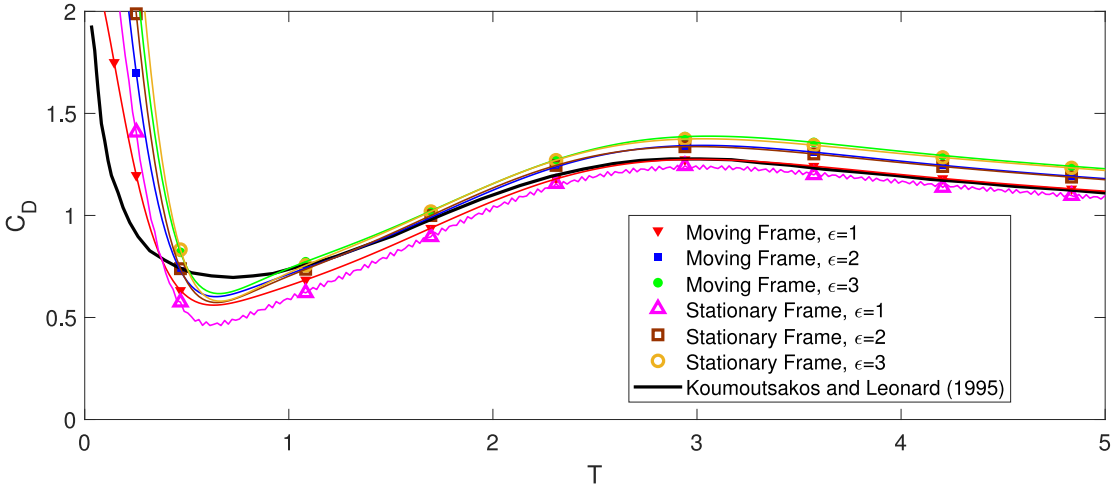

(b) C_D history of moving frame (solid markers) and stationary frame (hollow symbols) cases with biased difference ζ_α under different boundary thicknesses ($\epsilon = 1, 2, 3$).

Fig. 10. Force history of impulsively started cylinder in a channel. The solid black lines are the results obtained by Koumoutsakos and Leonard in 1995 [33]..

The following table shows the steady state C_D calculated DBB-LBM under different boundary thicknesses and resolutions.

Relevant published numerical and experimental data are also listed in the above Table 1. The results show that in most cases DBB-LBM can recover reasonable drag coefficients. From the results we see the drag coefficient at steady sate in general converges when boundary thickness is decreased. However, when boundary thickness is 1, the C_D value is a bit off the expectation. This can be caused by the lack of boundary nodes for integration. The drag coefficient value also converges as mesh is refined. Biased difference ζ_α as expected produces results closer to the reported data. Although open boundaries are employed to reduce the force fluctuations, inlet and outlet boundary effects can still be detected in the C_D history.

3.3. Flow past a impulsively started cylinder in a channel

This simulation is inspired by applications by Lallemand and Luo [4] and Lee and Lin [32]. The purpose of this simulation is to show the Galilean Invariance of DBB-LBM. The setup is similar to the 2D cylinder flow. Reynolds number here is 550. Time is normalised by $\Delta T = D/(2U)$. Different boundary thicknesses ($\epsilon = 1, 2, 3$) are applied to this application. The resolution is 4096 by 4096 and the characteristic length remains 64, so that force fluctuations caused by wall effects would not appear in the early time of simulation. In this application we consider two cases, moving frame and stationary frame. Left and right boundaries are periodic in both cases. In moving frame case, upper and lower walls moves to the right with a speed of U, and the cylinder is fixed at the center of the domain (Fig. 8a). In the stationary frame case, the walls are stationary, and starting from the center of the domain the cylinder moves to the left with a speed of U (Fig. 8b).

In this application we consider the transient solution for relatively high Reynolds number fluid. Since the distance from the cylinder to the inlet is changing for the stationary frame case, it is not mathematically perfectly identical to the moving frame case. Therefore we only consider the period $T = [0, 5]$ so that the inlet does not bring in too much boundary effect. Below are the streamlines when T is 1, 3 and 5. The upper halves are the moving frame solutions and the lower haves are the stationary frame solutions. (Fig. 9.)

As Lallemand and Luo have indicated in [4], the moving frame case and the stationary frame case should be decently identical. Fig. 9 shows such agreement for different stages of the evolution. The Galilean Invariance feature is also reflected by the drag coefficient. Fig. 10 shows the behavior of C_D for different cases.

Fig. 10a tracks the history of drag force in both stationary frame and moving frame cases with analytical ζ_α. For each boundary thickness, the evolutions of moving frame and stationary frame cases in general agree with each other. Obvious fluctuations can be detected in the stationary frame cases when boundary thickness is 1. This is typical sharp boundary effect and can be reduced by increasing the boundary thickness. At sharp boundary limit when real bounce back is recovered, the force fluctuation becomes prominent. An explanation of the fluctuation is that the physical properties of newly generated fluid nodes caused by particle motion are not correctly recovered. Although force fluctuations of the stationary frame case are not completely removed for narrow boundary cases, it is almost neglegible compared to force behaviors in [4]. Fig. 10b shows the drag force histories obtained by biased difference ζ_α. It is interesting to note that biased difference ζ_α not only produces more accurate physical properties, but also significantly mutes the noises when boundary is close to sharp limit.

4. Conclusions

The DBB-LBM proposed in this work is an implicit boundary scheme for LBM. It is inspired by the work of Li et al. [17] and Aland et al. [18]. The derivation starts from incorporating the bounce back boundary condition into the weak form of DBE. The derived equation is in continuous form and can be discretized into Implicit Euler and Crank-Nicolson schemes. Both schemes are independent of the collision process. This feature makes it easier to combine DBB-LBM with different collision models. Unlike many implicit boundary conditions, this new scheme is second order convergence. The accuracy is tested with Taylor-Couette flow benchmark problem. The accuracy of drag force is validated in 2D cylinder flow problem. Force accuracy also depends on the boundary thickness. We suggest that the boundary thickness be as small as possible, as far as the interface profile remains smooth. Large boundary thickness can make the boundary effect spread and therefore decrease the force accuracy. For implicit Euler case, our recommendation for the thickness value is 1 in lattice unit, and for Crank Nicolson case, it should be at least 2 for numerical stability reasons. Another benchmark problem of impulsively started cylinder flow inspired by Lallemand and Luo [4] is implemented to study the Galilean invariance error and the fluctuations caused by moving boundaries. The force fluctuation with DBB-LBM can be well controlled by applying diffuse boundary method.

Declaration of Competing Interest

The authors declare that they have no known competing financial interests or personal relationships that could have appeared to influence the work reported in this paper.

CRediT authorship contribution statement

Geng Liu: Validation, Software, Writing - original draft. **Taehun Lee:** Conceptualization, Supervision.

Acknowledgments

This research was supported by the National Science Foundation under Grant No. 1743794, PIRE: Investigation of Multi-Scale, Multi-Phase Phenomena in Complex Fluids for the Energy Industries.

References

[1] Filippova O, Hänel D. Grid refinement for lattice-BGK models. J Comput Phys 1998;147:219–28.
[2] Mei R, Shyy W, Yu D, Luo L-S. Lattice Boltzmann method for 3-D flows with curved boundary. J Comput Phys 2000;161(2):680–99.
[3] Bouzidi M, Firdaouss M, Lallemand PJ. Momentum transfer of a Boltzmann-lattice fluid with boundaries. J Comput Phys 2003;13(11):3452–9.
[4] Lallemand P, Luo L-S. Lattice Boltzmann method for moving boundaries. J Comput Phys 2003;184:406–21.
[5] Rohde M, Kandhai D, Derksen JJ, den Akker HEV. Improved bounce-back methods for no-slip walls in lattice-Boltzmann schemes: theory and simulations. Phys Rev E Stat Nonlin Soft Matter Phys 2003;67(6 Pt 2):066703.
[6] Mei R, Yu D, Shyy W, Luo L-S. Force evaluation in the lattice Boltzmann method involving curved geometry. Phys Rev E Stat Nonlin Soft Matter Phys 2002;65(4 Pt 1):041203.
[7] Peskin C. Numerical analysis of blood flow in the heart. J Comput Phys 1977;25:220–52.
[8] Peskin CS. The immersed boundary method. Acta Numer 2002;11:479–517.
[9] Feng Z-G, Michaelides EE. The immersed boundary-lattice Boltzmann method for solving fluid-particles interaction problems. J Comput Phys 2004;195(2):602–28.
[10] Feng Z-G, Michaelides EE. Proteus: a direct forcing method in the simulations of particulate flows. J Comput Phys 2005;202(1):20–51.
[11] Niu XD, Shu C, Chew YT, Peng Y. A momentum exchange-based immersed boundary-lattice Boltzmann method for simulating incompressible viscous flows. Phys Lett A 2006;354(3):173–82.
[12] Caiazzo A, Junk M. Boundary forces in lattice Boltzmann: analysis of momentum exchange algorithm. Comput Math Appl 2008;55(7):1415–23.

[13] Inamuro T. Lattice Boltzmann methods for moving boundary flows. Fluid Dyn Res 2012;44(2):024001.
[14] Noble DR, Torczynski JR. A lattice-Boltzmann method for partially saturated computational cells. Int J Mod Phys C 1998;9(8):1189–201.
[15] Zou Q, He X. On pressure and velocity boundary conditions for the lattice Boltzmann BGK model. Phys Fluids 1997;9:1591.
[16] Krause MJ, Klemens F, Henn T, Robin T, Nirschl H. Particle flow simulations with homogenised lattice Boltzmann methods. Particuology 2017;34:1–13.
[17] Li X, Lowengrub J, Rätz A, Voigt A. Solving PDEs in complex geometries: a diffuse domain approach. Commun Math Sci 2009;7(1):81–107.
[18] Aland S, Lowengrub J, Voigt A. Two-phase flow in complex geometries: a diffuse domain approach. Comput Model Eng Sci 2010;57(1):77–106.
[19] Lallemand P, Luo L-S. Theory of the lattice Boltzmann method: dispersion, dissipation, isotropy, galilean invariance, and stability. Phys Rev E Stat Phys Plasmas Fluids Relat Interdiscip Top 2000;61(6 Pt A):6546–62.
[20] Bhatnagar P, Krook EGM. A model for collision processes in gases. I. Small amplitude processes in charged and neutral one-component systems. Phys Rev 1954;94(3):511–25.
[21] Qian YH, d'Humieres D, Lallemand P. Lattice BGK models for Navier-Stokes equation. Europhys Lett 1992;17(6):479–84.
[22] He X, Luo L-S. Lattice Boltzmann model for the incompressible Navier-Stokes equation. J Stat Phys 1997;88:927–44.
[23] Zou Q, Hou S, Chen S, Doolen GD. An improved incompressible lattice Boltzmann model for time-independent flow. J Stat Phys 1995;81:35–48.
[24] Lin Z, Fang H, Tao R. Inproved lattice Boltzmann model for incompressible two-dimensional steady flow. Phys Rev E 1996;54:6323–30.
[25] JDellar P. An interpretation and derivation of the lattice Boltzmann method using Strang splitting. Comput Math Appl 2013;65(2):129–41.
[26] Patel S, Lee T. A new splitting scheme to the discrete Boltzmann equation for non-ideal gases on non-uniform meshes. J Comput Phys 2016;327:799–809.
[27] Tritton DJ. Experiments on the flow past a circular cylinder at low Reynolds numbers. J Fluid Mech 1959;6(4):547–67.
[28] Fornberg BA. A numerical study of steady viscous flow past a circular cylinder. J Fluid Mech 1980;98(4):819–55.
[29] Calhoun D. A cartesian grid method for solving the two-dimensional streamfunction-vorticity equations in irregular regions. J Comput Phys 2002;176(2):231–75.
[30] Nieuwstadt F, Keller H. Viscous flow past circular cylinders. Comput Fluids 1973;1:59.
[31] He XY, Luo L-S. A priori derivation of the lattice Boltzmann equation. Phys Rev E 1997;55:R6333.
[32] Lee T, Liu C-L. An Eulerian description of the streaming process in the lattice Boltzmann equation. J Comput Phys 2003;185:445–71.
[33] Koumoutsakos P, Leonard A. High-resolution simulations of the flow around an impulsively started cylinder using vortex methods. J Fluid Mech 1995;296:1–38.